operation, development, and application, Microwave Online Syst Company web site, 1996.
5. D.M. Pozar, Microstrip antennas, Proc IEEE 80 (1992), 79–91.
6. C.A. Balanis, Antenna theory: Analysis and design, 2nd ed., Wiley, New York, 1997, ch. 14.
7. D.M. Pozar and S.D. Targonski, Improved coupling for aperture-coupled microstrip antennas, Electron Lett 27 (1991), 1129–1131.
8. S.D. Targonski, R.B. Waterhouse, and D.M. Pozar, Wideband aperture-coupled microstrip patch array with backlobe reduction, IEE Electron Lett 33 (1997), 2005–2006.

A FAST 2D VOLUME INTEGRAL-EQUATION SOLVER FOR SCATTERING FROM INHOMOGENEOUS OBJECTS IN LAYERED MEDIA

Lin-Ping Song,[1,*] Ergün Şimşek,[2] and Qing H. Liu[2]
[1] University of British Columbia, Vancouver, Canada
[2] Department of Electrical and Computer Engineering
Duke University
Box 90291, Durham, NC 27708-0291

Received 4 April 2005

ABSTRACT: *The stabilized biconjugate gradient fast Fourier transform (BCGS-FFT) method is applied to simulate electromagnetic and acoustic scattering from inhomogeneous objects embedded in a layered medium in two dimensions. Two-dimensional layered-media Green's functions are computed adaptively by using Gaussian quadratures after singularity subtraction. The Green's function is split into convolutional and correlational components in order to apply the FFT so as to solve the scattering problem efficiently. The CPU time and memory cost of this BCGS-FFT method is $O(N \log N)$ and $O(N)$, respectively, where N is the number of unknowns, which is significantly more efficient than using the method of moments (MoM). As a result, this method is capable of solving large-scale electromagnetic and acoustic scattering problems for inhomogeneous objects embedded in a layered medium with an arbitrary number of layers.* © 2005 Wiley Periodicals, Inc. Microwave Opt Technol Lett 47: 128–134, 2005; Published online in Wiley InterScience (www.interscience.wiley.com). DOI 10.1002/mop.21101

Key words: *stabilized biconjugate gradient fast Fourier transform (BCGS-FFT) method; fast algorithm; layered media; scattering; volume integral equation*

1. INTRODUCTION

Electromagnetic and acoustic scattering from inhomogeneous objects of arbitrary shape embedded in a layered medium has been a very important research topic because of its wide application in areas such as geophysical exploration, remote sensing, biomedical imaging, landmine detection, underwater acoustics, interconnect simulations, microstrip antennas, and monolithic microwave integrated circuits. The complex background and the large number of unknowns associated with realistic targets make the problem more challenging. For both 2D and 3D cases, the development of fast algorithms for such complicated environment is still an intensive research topic.

For homogeneous objects embedded in a layered medium, surface integral equations (SIEs) are more appropriate than volume integral equations (VIE) [1–4, 37]. However, for inhomogeneous objects, the SIE must be combined with other methods such as the finite-element method in order to account for the inhomogeneity. A conventional method of solving the scattering problem for inhomogeneous objects is the method of moments (MoM), which discretizes the volume integral equation first and then solves the linear system with N unknowns, requiring $O(N^2)$ memory, and $O(KN^2)$ CPU time using an iterative solver, where K is the number of iterations [1–3, 5–7]. Another way of solving this problem is fast multipole method (FMM) which reduces the CPU time and memory requirements to $O(N \log N)$ [8–10]. With the presented method, the memory requirement and the computational cost are reduced to $O(N)$ and $O(KN \log N)$, respectively, making it highly suitable for large-scale problems.

The combination of iterative solvers with the fast Fourier transform (FFT) algorithm has been studied in detail for free-space scattering problems [11–22] and for electromagnetic wave-scattering problems in layered media [23–27]. Different from these works, a fast solver for 2D electromagnetic and acoustic wave scattering in layered media has been developed in this work. Although the 3D counterparts of this work have been published recently, no 2D BCGS-FFT method has been published for layered media with an arbitrary number of layers. In practical applications, it is desirable to have a fast simulation code for rapid data processing; therefore, it is worthwhile to develop such a fast solver for 2D applications.

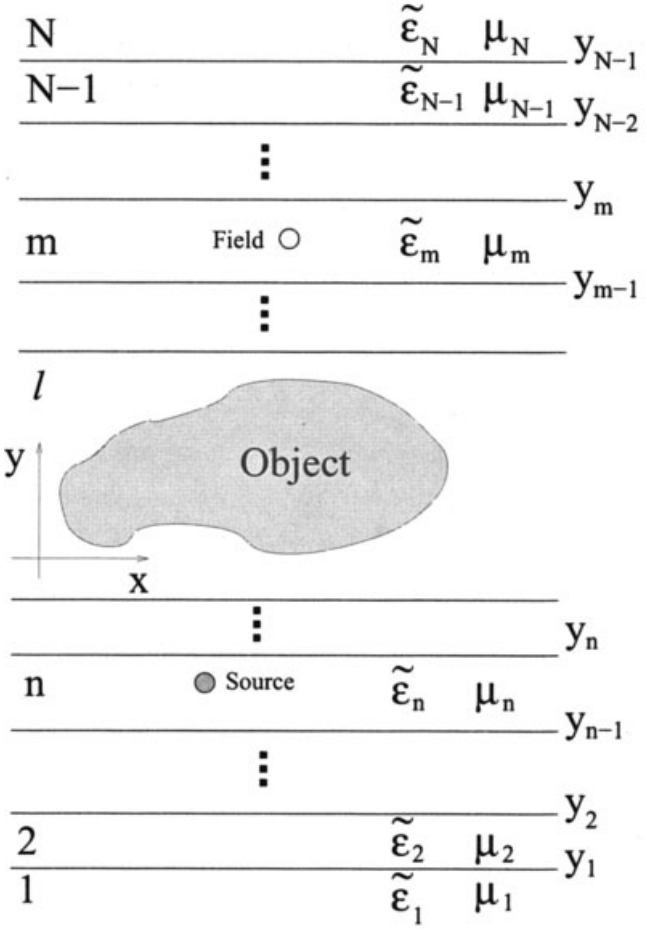

Figure 1 An N-layer medium with an object in layer l and source and field points in layers n and m, respectively. Layer i exists between y_i and y_{i-1} and is characterized by relative complex permittivity $\tilde{\epsilon}_{r,i}$ and relative permeability $\mu_{r,i}$

This work was supported by the National Science Foundation through grants CCR-00-98140 and IIS-0086075.
* Lin-Ping Song was formerly with Duke University.

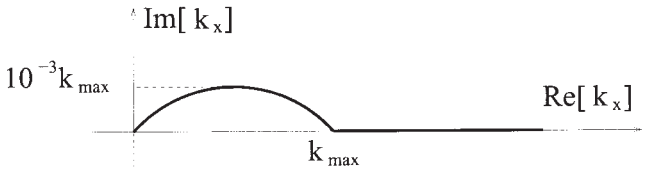

Figure 2 Deformed integration path in the complex k_x plane, $k_{\max} = 1.2 \max\{k_1, k_2, \ldots, k_N\}$

For the implementation of the 2D BCGS-FFT method for layered media, first, 2D layered-medium Green's functions are calculated. However, to be able to use FFT algorithms, the Green's functions are split into two terms to allow the electric-field integral-equation (EFIE) kernels to be evaluated via FFT by using convolution and correlation theorems. Finally, the linear system is solved by the stabilized biconjugate-gradient (BiCGSTAB) method. The CPU time and memory cost of this BCGS-FFT method are $O(N \log N)$ and $O(N)$, respectively, where N is the number of unknowns. However, at present, the inhomogeneous object must be located completely within one single layer in this multilayer medium, but efforts are underway to remove this limitation.

The outline of this paper is as follows. Firstly, the volume integral equation (VIE) for inhomogeneous objects embedded in layered media is briefly reviewed. Secondly, the splitting technique of 2D layered media Green's function is explained. Thirdly, the implementation of BCGS-FFT for 2D layered media is described. Finally, issues with regard to accuracy and efficiency of the method are studied via several numerical examples.

2. VOLUME INTEGRAL EQUATION FOR LAYERED MEDIA

Consider a general multilayer medium consisting of N layers separated by $N - 1$ interfaces parallel to the x axis, as shown in Figure 1. Layer i exists between y_i and y_{i-1} and is characterized by relative complex permittivity $\tilde{\varepsilon}_{r,i}$ and relative permeability $\mu_{r,i}$. The inhomogeneous object is assumed to be completely embedded in layer l. The objective here is to calculate the electromagnetic field due to a line source in such a complex medium.

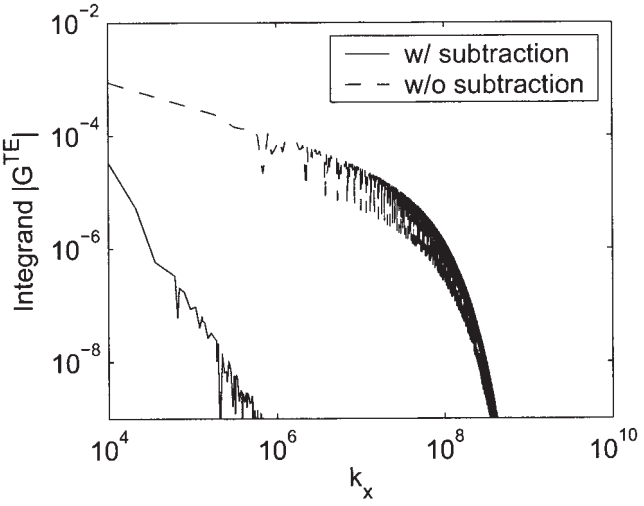

Figure 3 Comparison of the magnitude of the spectral-domain Green's function with and without primary field-term subtraction for a two-layer medium ($\varepsilon_{r,1} = 1$, $\varepsilon_{r,2} = 2$, interface at $y = 0$ m) with $y' = -y = \lambda/1000$

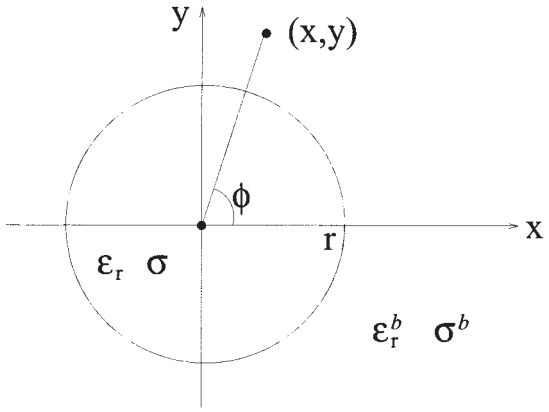

Figure 4 An infinite homogeneous-dielectric circular cylinder (radius r, relative permittivity $\tilde{\varepsilon}_r$, conductivity σ_i) with a homogeneous background (relative permittivity $\tilde{\varepsilon}_r^b$, conductivity σ^b)

For the TM$_z$ case, the total electric field, $E_{z,n}(\bar{\rho})$, in layer n is the sum of the incident field $E_{z,n}^{inc}(\bar{\rho})$ and the scattered field $E_{z,n}^{s}(\bar{\rho})$, given by

$$E_{z,n}^{inc}(\bar{\rho}) = E_{z,n}(\bar{\rho}) - E_{z,n}^{s}(\bar{\rho}), \tag{1}$$

where $\bar{\rho}$ is the position vector in the 2D space, and $E_{z,n}^{inc}(\bar{\rho})$ is the electric field in the absence of the object but with the presence of the layered medium.

The scattered field in the n^{th}-layer due to the induced current source, J_z, inside the inhomogeneous object embedded in the l^{th}-layer can be given by

$$E_{z,n}^{s}(\bar{\rho}) = -j\omega\mu_n \int_V G(\bar{\rho}, \bar{\rho}') J_z(\bar{\rho}') d\bar{\rho}'$$

$$= \omega^2 \mu_n \tilde{\varepsilon}_l \int_V G(\bar{\rho}, \bar{\rho}') \chi(\bar{\rho}') E_z(\bar{\rho}') d\bar{\rho}', \tag{2}$$

where $G(\bar{\rho}, \bar{\rho}')$ is the 2D Green's function to be explained next, V is the volume of the scattering object, $\chi(\bar{\rho}) = \tilde{\varepsilon}(\bar{\rho})/\tilde{\varepsilon}_l - 1$, is the contrast function, and the complex permittivity is defined as $\tilde{\varepsilon}(\bar{\rho}) = \varepsilon(\bar{\rho}) + \sigma(\bar{\rho})/j\omega$.

By substituting Eq. (2) into Eq. (1), we obtain

$$E_{z,n}^{inc}(\bar{\rho}) = E_{z,n}(\bar{\rho}) - k_n^2 \frac{\tilde{\varepsilon}_l}{\tilde{\varepsilon}_n} \int_V G(\bar{\rho}, \bar{\rho}') \chi(\bar{\rho}') E_{z,l}(\bar{\rho}') d\bar{\rho}'. \tag{3}$$

When $n = l$ and $\bar{\rho} \in V$, Eq. (3) can be written as an EFIE:

$$\mathcal{L}[E_{z,l}(\bar{\rho})] = E_{z,l}^{inc}(\bar{\rho}), \tag{4}$$

where $\mathcal{L}$ is a linear operator defined as

$$\mathcal{L}[\ ] = [\ ] - k_l^2 \int_V G(\bar{\rho}, \bar{\rho}') \chi[\ ] d\bar{\rho}'. \tag{5}$$

The induced current (or the electric field intensity, since $J_z = j\omega\tilde{\varepsilon}_l \chi E_z$) inside the scattering object can be calculated by solving

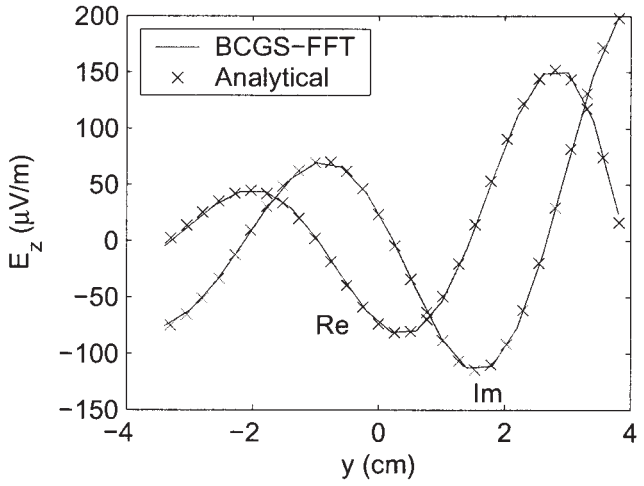

Figure 5 Comparison of the real and imaginary parts of the total field inside the lossy cylinder ($r = 0.04$ m, $\varepsilon_r = 57.2$, $\sigma_r = 1.08$ S/m) in a homogeneous background ($\varepsilon_r^b = 16$, $\sigma^b = 0.16$ S/m), shown in Fig. 4. The receivers are located at $(0, y)$, $y \in (-0.04, 0.04)$ m

(4). Hence, the electric field at any location can be easily obtained by using (2).

3. 2D GREEN'S FUNCTIONS

The formulation of the 2D Green's function is very similar to the 3D case, and the reader may refer to [3, 28] for the details of the derivation procedure of the multilayer media Green's functions in 3D.

Essentially, the evaluation process consists of two steps. The first step is the evaluation of the spectral-domain Green's function using a transmission-line analogy, in which each layer is represented by a uniform transmission line having the same physical properties; hence, the electric and magnetic fields are interpreted as voltage and current, respectively, on a transmission line. The second step is the inverse transformation from the spectral domain to the spatial domain, by evaluating the Sommerfeld integral [29], given by

$$G^p(x - x', y|y') = \frac{1}{2\pi}\int_{-\infty}^{\infty} \tilde{\tilde{G}}^p(k_x, y|y')\, e^{jk_x(x-x')}dk_x$$

$$= \frac{1}{\pi}\int_0^{\infty} \tilde{\tilde{G}}^p(k_x, y|y')\cos k_x(x - x')dk_x, \quad (6)$$

where $k_x^2 = k^2 - k_y^2$, and $G^p(x - x', y|y')$ is a p type (p is either TE or TM) Green's function relating the field at (x, y) in layer m due to a unit source at (x', y') in layer n, and $\tilde{G}^p$ and its spectral-domain counterpart, which has a closed-form expression depending on the locations of the source and field points:

$$\tilde{\tilde{G}}^{TE} = \frac{1}{j\omega\mu_m}\tilde{G}_{mn}^{TE}(k_x, y|y'), \quad (7)$$

$$\tilde{\tilde{G}}^{TM} = \frac{1}{j\omega\tilde{\varepsilon}_n}\tilde{G}_{mn}^{TM}(k_x, y|y'). \quad (8)$$

For the details of the expressions of $\tilde{\tilde{G}}^{TE}$ and $\tilde{\tilde{G}}^{TM}$, the reader is referred to [28].

It is well known that the integrand in Eq. (6) has pole singularities and branch cuts on the real k_x axis from $k_x = 0$ to $k_x = k_{\max}$, where $k_{\max} = \max\{k_1, k_2, \ldots, k_N\}$. For the 3D case, it is shown that the efficiency of the numerical integration can be improved by deforming the integration path in the complex k_ρ plane [30]. By using the same idea, the integration can be performed on the deformed Sommerfeld integration path, as depicted in Figure 2.

When the source and field points are in the same layer, a primary field term can be subtracted from the integrand, as it is done for 3D case, by using the following equation:

$$\frac{1}{2\pi}\int_0^{\infty} \frac{e^{-jk_{y,m}|y-y'|}}{jk_{y,m}}\cos k_x(x - x')dk_x$$

$$= \frac{j}{4}H_0^{(1)}(k_m\sqrt{(x - x')^2 + (y - y')^2}). \quad (9)$$

For the fast convergence of the Sommerfeld integral, we use this singularity subtraction, even when the field point is in a different layer than the source point [31]. This procedure significantly increases the speed of the evaluation process, especially for cases where the source and field points are near an interface of two adjacent layers. Figure 3 shows a comparison of the magnitude of the spectral-domain Green's function with and without the singularity subtraction for a 2-layer medium problem ($\varepsilon_{r,1} = 1$, $\varepsilon_{r,2} = 2$, and the interface is at $y = 0$ m) and $y' = -y = \lambda/1000$. As can be seen from the figure, after subtraction the integrand becomes a rapidly decreasing function of k_x. In fact, this decaying process is exponential, and is five orders of magnitude smaller than the original integrand at $k_x = 10^5$.

Note that the Green's functions are shift-invariant in the x direction but not in the y direction. As a result, the convolutional theorem cannot be used directly to arrive at the FFT acceleration in the CG-FFT, BCG-FFT, and BCGS-FFT methods as in the case of a homogeneous background. However, similar to the 3D case [19–27], the 2D Green's function can be written as a summation of two terms as follows:

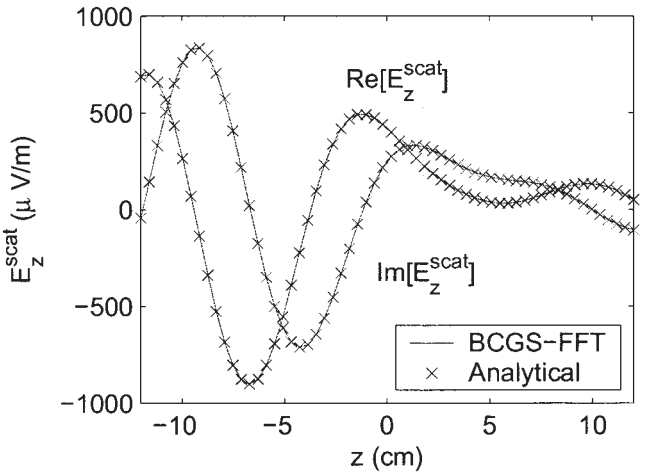

Figure 6 Comparison of BCGS-FFT and the analytical results for the real and imaginary parts of the scattered field from a lossy cylinder ($r = 0.05$ m, $\varepsilon_r = 8.0$, $\sigma_r = 0.2$ S/m) in a homogeneous background ($\varepsilon_r^b = 4.0$, $\sigma_r^b = 0.01$ S/m), as shown as Fig. 4. The receivers are at $(0.08, y)$, $y \in (-0.12, 0.12)$ m

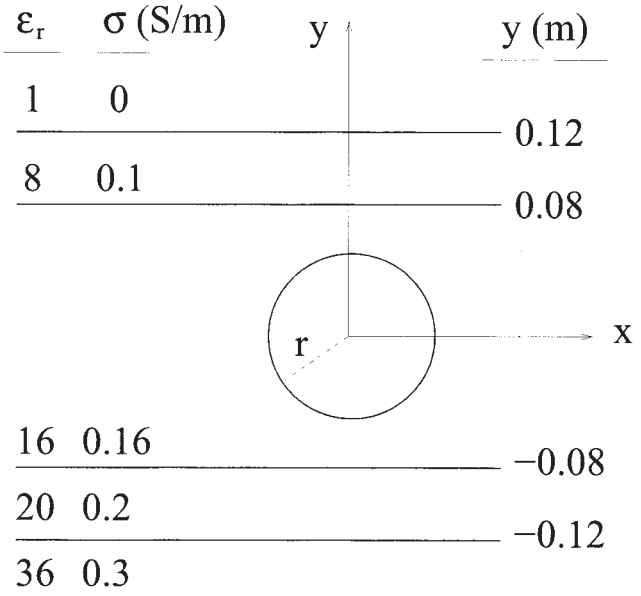

Figure 7 A lossy cylinder ($r = 0.05$ m, $\varepsilon_r = 57.2$, $\sigma_r = 1.08$ S/m) embedded in a five-layer media. The center of the object is located at origin, the line source is located at (0, 0.15) m, and $f = 900$ MHz

$$G(\bar{\rho}, \bar{\rho}') = G_1(|x - x'|, y - y') + G_2(|x - x'|, y + y'). \quad (10)$$

Clearly, $G_1(|x - x'|, y - y')$ is shift-invariant in both x and y directions; $G_2(|x - x'|, y + y')$ is shift-invariant in x direction and is a function of $y + y'$ in the y direction. As a result, in (5), the interaction between $G_1(\bar{\rho}, \bar{\rho}')$ and $\chi(\bar{\rho}')E_z(\bar{\rho}')$ is a convolution in both (x, y) directions, and that between $G_2(\bar{\rho}, \bar{\rho}')$ and $\chi(\bar{\rho}')E_z(\bar{\rho}')$ is a convolution in the x direction and a correlation in the y direction. In other words, the integral kernel in the EFIE is convolutional in the x direction and convolutional or correlational in y the direction after the splitting. Consequently, the FFT can be applied to these two operations separately through the convolution and correlation theorems, reducing CPU time of the "Green's operation" from $O(N^2)$ to $O(N \log N)$.

4. ITERATIVE SOLVER AND COMPUTATIONAL COST

A discrete linear system can be obtained from the EFIE of Eq. (4) by using Galerkin's method. In this paper, both the basis and testing functions are rooftop functions. After discretization, the convolution and correlation kernels in the EFIE are transformed into discrete convolution and correlation kernels. Using the convolution and correlation theorems, these discrete convolution and correlation can be performed efficiently by using the FFT algorithm. For each Bi-CGSTAB iteration, the $\mathcal{L}$ operation costs $O(N \log N)$ arithmetic operations. The total computational cost of the BCGS-FFT method is $O(K\,N \log N)$, where K is the number of iterations [32–36]. On the other hand, the MoM matrix does not have to be stored. To perform the $\mathcal{L}$ operation, only a few vectors of dimension N are required; hence, the memory requirement is $O(N)$.

5. EXTENSION TO 2D ACOUSTIC SCATTERING IN A LAYERED MEDIUM

The extension of this BCGS-FFT method to the acoustic case is trivial as the 2D acoustic equation is the same as the TM_z case, with μ and $k = \omega\sqrt{\mu\tilde{\varepsilon}}$ being replaced by ρ (mass density) and $k = \omega/c$ (c is the acoustic velocity), respectively. In this case, we assume there is no contrast in ρ between the object and layer l; however, the mass density for all layers can be different.

6. NUMERICAL RESULTS

In this paper, the source is chosen as a z-directed electric-line source appropriate for near-field applications such as microwave imaging and landmine detection. The method can be also used for far-field applications such as remote-sensing and radar technologies, simply by using plane-wave incidence instead of a line source. To be able to show the accuracy and efficiency of the method, several examples are presented below.

6.1. Homogeneous Object/Homogeneous Background

In the first example, a large-contrast circular cylinder ($\varepsilon_r = 57.2$, $\sigma_r = 1.08$ S/m, and a diameter of 0.08 m) is simulated in a homogeneous background ($\varepsilon_r^b = 16$, and $\sigma_r^b = 0.16$ S/m), as depicted in Figure 4. The line source is located at (0, 0.12) m and has a frequency $f = 800$ MHz. The electric field inside the cylinder is computed with the described BCGS-FFT method for observation points at $(0, y)$, $y \in (-0.04, 0.04)$ m. Figure 5 shows a comparison of the numerical result and the analytical solution. Both the real and imaginary parts of the numerical result agree well with the analytical solution.

The second example is similar to the first one; however, in this case the chosen observation points are outside the cylinder. The background properties are $\varepsilon_r^b = 4.0$ and $\sigma_r^b = 0.01$ S/m. The lossy cylinder (radius $r = 0.05$ m, $\varepsilon_r = 8.0$, and $\sigma_r = 0.2$ S/m) is excited by a line source located at $(-0.12, 0.12)$ m, while the observation points are at $(0.08, y)$, $y \in (-0.12, 0.12)$ m and $f = 2$ GHz. Figure 6 shows the excellent agreement between the numerical result and the analytical solution.

6.2. Homogeneous Object/Layered Medium

The third example involves an infinite circular dielectric cylinder embedded in a five-layer medium. Each layer has different permittivity and thickness, as depicted in Figure 7. The line source is located at (0.0, 0.15) m, and the object is embedded in the third layer, centered at the origin, with $r = 0.05$, $\varepsilon_r = 57.2$, and $\sigma = 1.08$ S/m; $f = 900$ MHz.

Figure 8 compares the field inside the object calculated with this method and the spectral integral method (SIM) for layered media [37]. The observation points are chosen at $x = 0$ (along the

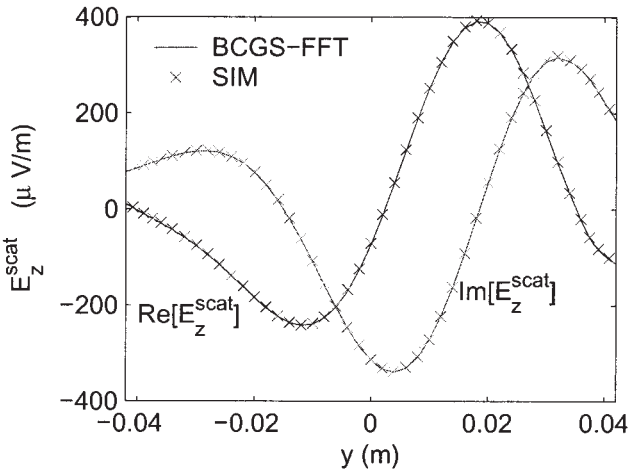

Figure 8 The scattered field inside the scatterer along (0.0:−0.042.0.042) m for the circular dielectric object in a five-layer medium depicted in Fig. 7

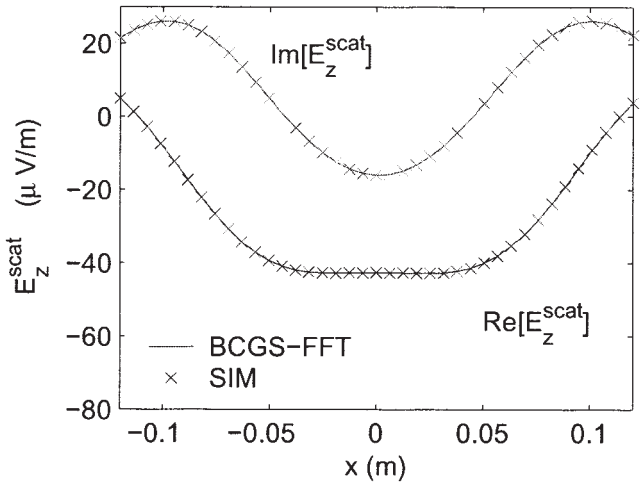

Figure 9 The scattered field along (−0.12:0.12,0.15) m for the circular dielectric object in a five-layer medium depicted in Fig. 7

y axis) from $y = -0.042$ m to $y = 0.042$ m. Excellent agreement between the VIE and SIM results is observed.

Figure 9 shows the comparison of the scattered field outside the object (in the first layer) calculated using the VIE and SIM. The observation points are located at $y = 0.15$, from $x = -0.12$ m to $x = 0.12$ m.

Figure 10 shows the comparison of scattered field at $x = 0.06$ m, from $y = -0.15$ m to $y = 0.15$ m (from the first layer to the last one). Both the VIE and SIM results show continuous field distribution across the layer interfaces, as expected.

The error versus iteration number for the above three examples is shown in Figure 11. Clearly, twelve iterations guarantee an error smaller than 0.1%.

6.3. Inhomogeneous Object/Homogeneous Background

In the fourth example, an infinite layered-dielectric circular cylinder centered at the origin is excited with a line source ($f = 800$ MHz) located at (0, 0.12) m in a homogeneous background ($\varepsilon_r^b = 16$, and $\sigma_r^b = 0.16$ S/m), as shown in Figure 12. The properties of the concentric cylinders are as follows:

$$r_1 = 0.01 \text{ m}, \varepsilon_{r,1} = 30.2, \sigma_1 = 0.02 \text{ (S/m)},$$

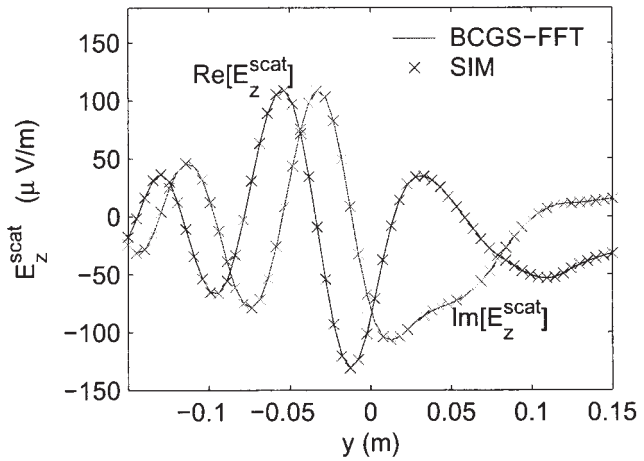

Figure 10 The scattered field along (0.06, −0.15:0.15) m, for the circular dielectric object in a five-layer medium depicted in Fig. 7

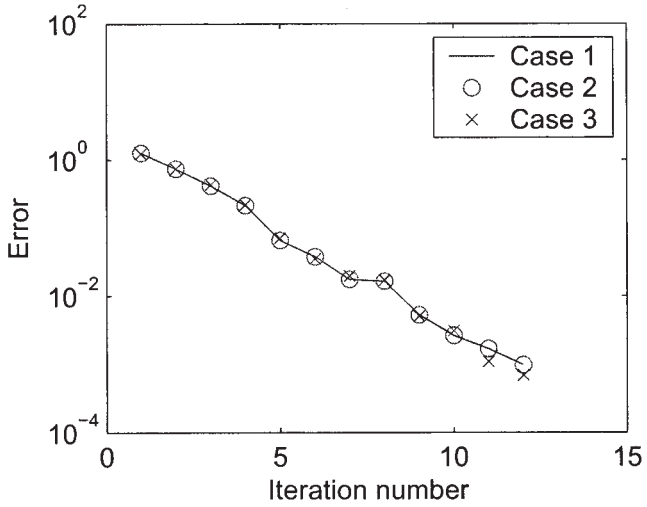

Figure 11 Error vs. iteration number for the circular dielectric object in a five-layer medium test. Case 1: receivers are inside the scatterer (Fig. 8). Case 2: receivers are in the first layer (Fig. 9). Case 3: receivers are from first layer to the last layer (Fig. 10)

$$r_2 = 0.02 \text{ m}, \varepsilon_{r,2} = 40.2, \sigma_2 = 0.08 \text{ (S/m)},$$

$$r_3 = 0.03 \text{ m}, \varepsilon_{r,3} = 50.2, \sigma_3 = 1.00 \text{ (S/m)},$$

$$r_4 = 0.04 \text{ m}, \varepsilon_{r,4} = 57.2, \sigma_4 = 1.08 \text{ (S/m)}.$$

Figure 13 shows the total field at (0, y), for $y \in (-0.05, 0.05)$ m.

6.4. Inhomogeneous Object/Layered Medium

Finally, the four-layer cylinder used in the previous example is embedded in the bottom layer of a three-layer medium, as shown in Figure 14, where the properties of the layers are also given. The line source is located (0, 0.12) m and $f = 800$ MHz. Figure 15 shows the total field, E_z, at (0, y), $y \in (-0.05, 0.05)$ m.

7. DISCUSSIONS AND CONCLUSION

The above examples are shown to demonstrate the application of the BCGS-FFT method for 2D electromagnetic waves for TM_z

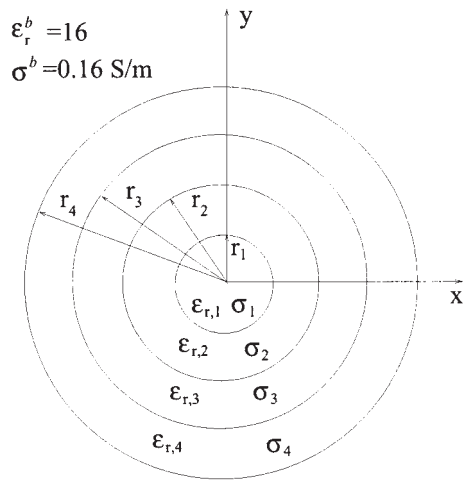

Figure 12 A four-layer dielectric circular cylinder in a homogeneous background. $r_i = (0.01, 0.02, 0.03, 0.04)$ m, $\varepsilon_{r,i} = (30.2, 40.2, 50.2, 57.2)$, and $\sigma_i = (0.02, 0.08, 1.0, 1.08)$ (S/m), where $i = 1, 2, 3, 4$. $\varepsilon_r^b = 16$ and $\sigma^b = 0.16$ S/m

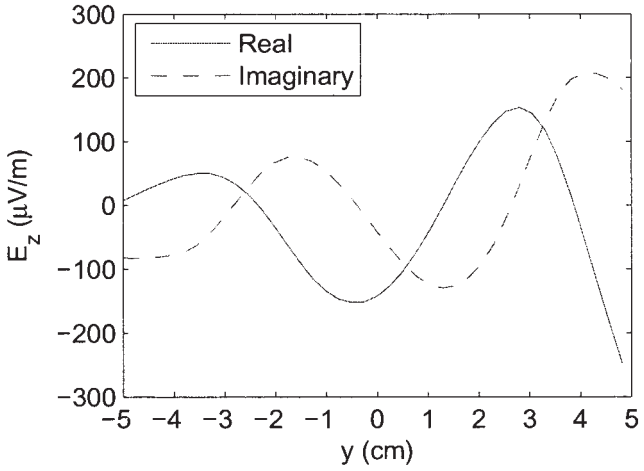

Figure 13 The real and imaginary parts of the total field at $(0, y)$, $y \in (-0.05, 0.05)$ m, for the four-layer dielectric cylinder in a homogeneous background shown in Fig. 12

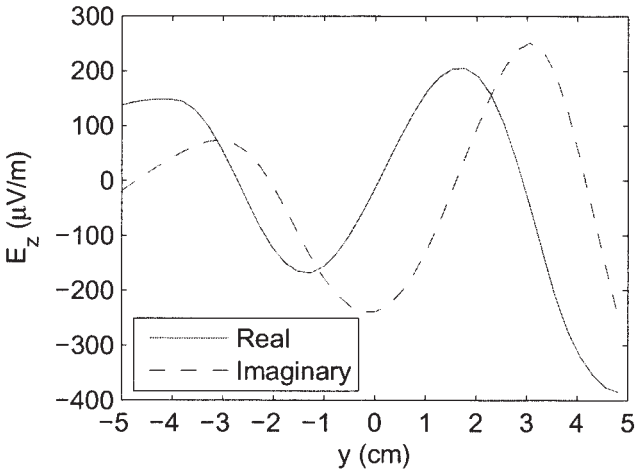

Figure 15 The real and imaginary parts of the total field at $(0, y)$, $y \in (-0.05, 0.05)$ m for the layered dielectric cylinder in a three-layer medium shown as Fig. 14

polarization. As mentioned above, the solver is directly applicable to acoustic waves. At present, the permeability (or mass density for acoustics) of the inhomogeneous object must be same as that in the layer where the object is embedded. However, all layers can have different permeability (for electromagnetics) or mass density (for acoustics).

A fast 2D solver for inhomogeneous objects embedded in multilayer media has been developed. A stabilized biconjugate-gradient iterative solver has been combined with fast Fourier transform for 2D layered media scattering problems. The CPU time of this method is $O(N \log N)$ and the memory cost is $O(N)$, making the method an ideal choice for large-scale problems. At present, the object must be embedded completely within one single layer in the multilayer medium, but efforts are underway to remove this limitation. This method can be combined with inverse-scattering problems and further extended to periodic layered-medium problems.

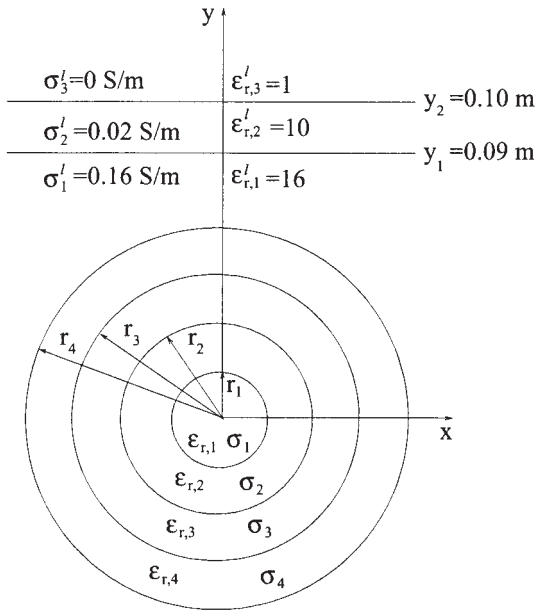

Figure 14 An infinite layered-dielectric circular cylinder in a three-layer media. The properties of the layered cylinders are same as those depicted in Fig. 12

REFERENCES

1. K.A. Michalski and D. Zheng, Electromagnetic scattering and radiation by surface of arbitrary shape in layered media part I: Theory, IEEE Trans Antennas Propagat 38 (1990), 335–344.
2. K.A. Michalski and D. Zheng, Electromagnetic scattering and radiation by surface of arbitrary shape in layered media part II: Implementation and results for contiguous half-space, IEEE Trans Antennas Propagat 38 (1990), 344–352.
3. K.A. Michalski and J.R. Mosig, Multilayered media Green's functions in integral equation formulations, IEEE Trans Antennas Propagat 45 (1997), 508–519.
4. E. Simsek and Q.H. Liu, Fast computation of dyadic Green's function for layered media and its application in interconnect simulations, IEEE Antennas Propagat Soc Symp Dig 3 (2004), 2783.
5. N. Geng and L. Carin, Wide-band electromagnetic scattering from a dielectric BOR buried in a layered lossy dispersive medium, IEEE Trans Antennas Propagat 47 (1999), 610–619.
6. Y. Liu, L.W. Li, T.S. Yeo, and M.S. Leong, Application of DCIM to MPIE-MoM analysis of 3D PEC objects in multilayered media, IEEE Trans Antennas Propagat 50 (2002), 157–162.
7. E. Jorgensen, O.S. Kim, P. Meincke, and O. Breinbjerg, Higher-order hierarchical discretization scheme for surface integral equations for layered media, IEEE Trans Geosci Remote Sensing 42 (2004), 764–772.
8. L. Gurel and M.I. Aksun, Electromagnetic scattering solution of conducting strips in layered media using the fast multipole method, IEEE Microwave Guided Wave Lett 6 (1996), 277–279.
9. B. Hu and W.C. Chew, Fast inhomogeneous plane wave algorithm for scattering from objects above the multilayered medium, IEEE Trans Geosci Remote Sensing 39 (2001), 1028–1038.
10. J. He, A. Sullivan, and L. Carin, Multilevel fast multipole algorithm for three-dimensional dielectric targets in the vicinity of a lossy half-space, Microwave Opt Technol Lett 29 (2001), 100–104.
11. M.F. Catedra, E. Gago, and L. Nuno, A numerical scheme to obtain the RCS of three-dimensional bodies of resonant size using the conjugate gradient method and the fast Fourier transform, IEEE Trans Antennas Propagat 37 (1989), 528–537.
12. P. Zwamborn and P.M. van den Berg, The three-dimensional weak form of the conjugate gradient FFT method for solving scattering problems, IEEE Trans Microwave Theory Tech 9 (1992), 1757–1766.
13. C.C. Su, The three-dimensional algorithm of solving the electric field integral equation using face-centered node points, conjugate gradient method, and FFT, IEEE Trans Microwave Theory Tech 41 (1993), 510–515.

14. H. Gan and W.C. Chew, A discrete BCG-FFT algorithm for solving 3D inhomogeneous scatter problems, J Electromagn Waves Applic 9 (1995), 1339–1357.
15. Z.Q. Zhang and Q.H. Liu, Three-dimensional weak-form conjugate and biconjugate-gradient FFT methods for volume integral equations, Microwave Opt Technol Lett 29 (2001), 350–356.
16. Z.Q. Zhang, Q.H. Liu, and X.M. Xu, RCS computation of large inhomogeneous objects using a fast integral equation solver, IEEE Trans Antennas Propagat 51 (2003), 613–618.
17. T.J. Cui and W.C. Chew, Novel diffraction tomographic algorithm for imaging two-dimensional dielectric objects buried under a lossy earth, IEEE Trans Geosci Remote Sensing 38 (2000), 2033–2041.
18. T.J. Cui, W.C. Chew, A.A. Aydiner, S.Y. Chen, D.L. Wright, D.V. Smith, J.D. Abraham, and R.T. Smith, Inverse scattering of 2D dielectric objects buried in a lossy earth using the distorted Born iterative method, IEEE Trans Geosci Remote Sensing 39 (2001).
19. J.W. Wiskin, D.T. Borup, and S.A. Johnson, Inverse scattering from arbitrary two-dimensional objects in stratified environments via a Green's operator, J Acoust Soc Am 102 (1997), 853–864.
20. T.J. Cui and W.C. Chew, Fast algorithm for electromagnetic scattering by buried 3-D dielectric objects of large size, IEEE Trans Geosci Remote Sensing 37 (1999), 2597–2608.
21. X.M. Xu and Q.H. Liu, The BCGS-FFT method for electromagnetic scattering from inhomogeneous objects in a layered medium, IEEE Antennas Wireless Propagat Lett 1 (2002), 77–80.
22. M.F. Catedra, E. Gago, and L. Nuno, A numerical scheme to obtain the RCS of three-dimensional bodies of resonant size using the conjugate gradient method and the fast Fourier transform, IEEE Trans Antennas Propagat 37 (1989), 528–537.
23. X.M. Xu, Q.H. Liu, and Z.Q. Zhang, The stabilized biconjugate gradient fast Fourier transform method for electromagnetic scattering, J Appl Comput Electromag Soc 17 (2002), 97–103.
24. X.M. Xu and Q.H. Liu, The BCGS-FFT method for electromagnetic scattering from inhomogeneous objects in a planarly layered medium, IEEE Antennas Wireless Propagat Lett 1 (2002), 77–80.
25. X. Millard and Q.H. Liu, A fast volume integral equation solver for electromagnetic scattering from large inhomogeneous objects in layered media, IEEE Trans Antennas Propagat 51 (2003), 2393–2401.
26. X. Millard and Q.H. Liu, Simulation of near-surface detection of objects in layered media by the BCGS-FFT method, IEEE Trans Antennas Propagat 42 (2004), 327–334.
27. F. Li, Q.H. Liu, and L.P. Song, Three-dimensional reconstruction of objects buried in layered media using Born and distorted Born iterative methods, IEEE Geosci Remote Sensing Lett 1 (2004), 107–111.
28. W.C. Chew, Waves and fields in inhomogeneous media, IEEE Press, Piscataway, NJ, 1995.
29. A. Sommerfeld, Partial differential equations, Academic, New York, 1949.
30. M. Paulus, P. Gay-Balmaz, and O.J.F. Martin, Accurate and efficient computation of the Green's tensor for stratified media, Physical Review, 62 (2000), 5797–5807.
31. E. Simsek, Q.H. Liu, and B. Wei, Singularity subtraction for evaluation of Green's functions for multilayer media, Submitted.
32. H.A. van der Vorst, Bi-CGSTAB: a fast and smoothly converging variant of Bi-CG for the solution of nonsymmetric linear systems, SIAM J Sci Stat Comput 13 (1992), 631–644.
33. M.R. Hestenes and E. Stiefel, Methods of conjugate gradients for solving linear systems, J Res Nat Bur Stand 49 (1952), 409–435.
34. T.K. Sarkar, On the application of the generalized biconjugate gradient method, J Electromagn Waves Appl 1 (1987), 223–242.
35. P. Sonneveld, CGS: a fast Lanczos-type solver for nonsymmetric linear system, SIAM J Sci Statist Comput 10 (1989), 36–52.
36. R.W. Freund, A transpose-free quasi-minimal residual algorithm for non-Hermitian linear systems, SIAM J Sci Comput 14 (1993), 470–482.
37. E. Simsek, J. Liu, and Q.H. Liu, A spectral integral method for layered media, Submitted.

A NEW MICROWAVE HARMONIC DIRECTION-FINDING SYSTEM FOR LOCALIZATION OF SMALL MOBILE TARGETS USING PASSIVE TAGS

E. de Moura Presa, J-F. Zürcher, and A. K. Skrivervik
Ecole Polytechnique Fédérale de Lausanne (EPFL)
Laboratoire d'Electromagnétisme et d'Acoustique
CH-1015 Lausanne, Switzerland

Received 20 April 2005

ABSTRACT: *A new harmonic direction-finding (HDF) system has been designed for the localization of small mobile targets using a radio-frequency identification (RFID) technique. Thanks to sophisticated electronics and high-performance filters and antennas, the system has a long range, despite the very small size of the passive tags placed on the targets. This and a very reduced weight are essential requirements for use with living targets such as small animals. Furthermore, it uses inexpensive electronics components and has autonomy on standard rechargeable batteries.* © 2005 Wiley Periodicals, Inc. Microwave Opt Technol Lett 47: 134–137, 2005; Published online in Wiley InterScience (www.interscience.wiley.com). DOI 10.1002/mop.21102

Key words: *harmonic radar; mobile targets; localization of small animals; passive tags; RFID; HDF*

1. INTRODUCTION

Within the frame of a research project [1, 2] in collaboration with the Laboratory for Conservation Biology of the University of Lausanne, our laboratory developed a microwave system allowing the localization of tree frogs. The principle chosen was to use miniaturized passive tags (transponders) placed on the frogs, made of an antenna and a frequency-doubling diode, which are to be localized by a transceiver. This idea can be equally applied to any small mobile target where the size and weight of the tag are of utmost relevance. The transceiver (HDF) consists of a transmitter working at 2.45 GHz with an output power of more than 1 W, and a high-sensitivity receiver at the double frequency (4.9 GHz). A specially designed antenna [3] has been specifically studied for this application, with high decoupling between both ports. This paper describes the transceiver (HDF) [4], which has been developed for this application.

2. DESCRIPTION OF THE TRANSCEIVER

Many possibilities exist for the development of such a transceiver. After a careful selection, taking into account parameters such as simplicity, performances, cost, availability of components, and so on, the architecture shown in Figure 1 was chosen.

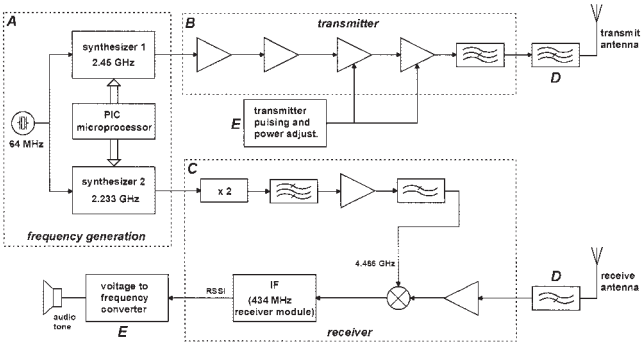

Figure 1 Schematic drawing of the complete HDF transceiver